tvst

https://doi.org/10.1167/tvst.8.3.16

Article

Detection of Malignancy in Ocular Surface Lesions by Inverse Spectroscopic Optical Coherence Tomography and Two-Photon Autofluorescence

Hyunjoo Jean Lee[1], Lei Zhang[2], Sui Zhang[3], and Ji Yi[2]

[1] Department of Ophthalmology, Boston Medical Center, Boston University School of Medicine, Boston, MA, USA
[2] Department of Medicine, Gastroenterology Section, Boston Medical Center, Boston University School of Medicine, Boston, MA, USA
[3] Dana Faber Cancer Institute, Boston, MA, USA

Correspondence: Hyunjoo Jean Lee, 85 E Concord St, 8th floor, Boston, MA 02118, USA. e-mail: Hyunjoo.Lee@BMC.org

Received: 15 August 2018
Accepted: 11 February 2019
Published: 8 May 2019

Keywords: inverse spectroscopic optical coherence tomography; OCT; auto-fluorescence; two-photon microscopy; ocular surface; OSSN; conjunctival tumors

Citation: Lee HJ, Zhang L, Zhang S, Yi J. Detection of malignancy in ocular surface lesions by inverse spectroscopic optical coherence tomography and two-photon autofluorescence. Trans Vis Sci Tech. 2019;8(3):16, https://doi.org/10.1167/tvst.8.3.16

Purpose: Advanced imaging is increasingly important in the diagnosis of ocular surface malignancy. Inverse spectroscopic optical coherence tomography (ISOCT) and two-photon autofluorescence microscopy (2P-AF) are emerging techniques capable of quantifying ultrastructural and metabolic changes, respectively. We aimed to detect malignancy in ocular surface lesions using ISOCT and 2P-AF.

Methods: Portions of excised specimens from patients undergoing conjunctival biopsy at Boston Medical Center were imaged by ISOCT and/or 2P-AF, and submitted for histologic diagnosis. Lesions were categorized as malignant, premalignant (with dysplasia) or benign. ISOCT and 2P-AF findings were compared between categories.

Results: Fourteen specimens from 13 patients were collected. The IS-OCT marker D was 2.2-fold higher in combined malignant and premalignant (4.27 ± 0.28, $n = 3$) versus benign (1.92 ± 0.26, $n = 11$) lesions ($P = 9 \times 10^{-4}$). ISOCT markers μ_s and μ_b were not significantly different. By 2P-AF, the redox ratio was 0.24-fold lower in premalignant (0.11 ± 0.004, $n = 2$) versus benign (0.45 ± 0.04, $n = 9$) lesions ($P = 1.08 \times 10^{-5}$).

Conclusions: Conjunctival lesions with higher malignant potential had higher D and lower redox ratios. Higher D can correlate with ultrastructural changes associated with malignancy, similar to what has been seen in cancers of the gut mucosa. Lower redox ratios can suggest the presence of the Warburg effect, which is associated with tumorigenesis.

Translational Relevance: IS-OCT and 2P-AF can potentially be applied to the detection of malignancy or malignant potential in ocular surface lesions. ISOCT allows for the detection of nanoscale ultrastructural changes that are not resolvable by conventional OCT.

Introduction

Conjunctival and corneal tumors comprise a broad array of benign, premalignant, and malignant neoplasms. Nevus, ocular surface squamous neoplasia (OSSN), primary acquired melanosis (PAM), and melanoma were the four most common diagnoses associated with referral to a large United States tertiary ocular oncology center, in descending order of frequency.[1] Distinguishing between benign and malignant lesions is not always straightforward,[2,3] and yet it is critical to making correct clinical treatment decisions. Reliable noninvasive diagnosis of ocular surface lesions is becoming particularly important as medical therapies have been effective for select types of tumors.[4,5] In particular, topical interferon-α2b has become a first-line therapy for the treatment of OSSN.[6,7] However, treating ocular surface tumors without surgical biopsy means that the diagnosis hinges on characterizing clinical features of the lesion, and observing its response to medical therapy. Misdiagnosis of a lesion could lead to delay of appropriate therapy.

There is increasing interest in clinical tools to aid in the diagnosis of ocular surface tumors, to help make preliminary diagnoses of lesions to help guide treatment decision. Impression cytology, a minimally-invasive way of harvesting superficial ocular surface cells for histology, has been used to distinguish benign from malignant lesions.[8,9] Imaging devices have been studied for their ability to improve the noninvasive detection and diagnosis of ocular surface pathology. Perhaps the most established and most widely available of these tools is anterior segment optical coherence tomography (AS-OCT). In particular, ultra-high resolution OCT (UHR-OCT) has the ability to help distinguish OSSN from benign lesions, such as pterygium, based on the characteristic appearance of full-thickness hyper-reflectivity of the involved epithelium in OSSN lesions with an abrupt transition to normal epithelium in uninvolved areas.[10–12] However, one cannot visualize differences in intracellular or ultrastructural characteristics with UHR-OCT. Thus, premalignant changes, such as cellular atypia associated with PAM, are not detectable by even the highest resolution spectral-domain OCT (SD-OCT) devices.[13,14]

Inverse spectroscopic OCT (ISOCT) is an emerging technology using SD-OCT signal re-sampling to determine the backscatter intensity spectra at every voxel in a three-dimensional (3D) OCT scan.[15] Specifically, by assuming tissue to be a continuous random medium, a mass density correlation parameter, D, can be obtained.[16] The higher D is, the greater the degree of tissue or cellular compaction. A unique feature of ISOCT is that the spectral analysis can sense the nanoscale structural modifications down to approximately 30 to 40 nm without the need to resolve the nanoarchitecture, while using OCT as a guide to locate the anatomic regions of interest. A previous study of ex vivo biopsies from colorectal and pancreatic cancer patients found that D was increased in tissues from these patients compared to normal controls, and suggested that ISOCT was sensitive for the detection of premalignant changes at an ultrastructural level, occurring below the optical diffraction limit.[17]

Two-photon autofluorescence microscopy (2P-AF) is another emerging technology that has allowed the evaluation of cellular metabolism in tissues by quantifying nicotinamide adenine dinucleotide (NADH) and flavin adenine dinucleotide (FAD) intrinsic autofluorescence to determine an optical redox ratio.[18] A decrease in the optical redox ratio is seen in states of increased glucose catabolism relative to oxidative phosphorylation, and can be associated with cancer, increased proliferation, or the process of cellular differentiation.[18]

Due to the potential ability of ISOCT and 2P-AF to aid in the differential diagnosis of benign, premalignant, and malignant lesions, we sought to apply these imaging techniques to ocular surface lesions. We describe the novel application of ISOCT and 2P-AF in quantifying ultrastructural and metabolic differences, respectively, between lesions of different malignant potential.

Methods

Human Subjects and Tissues

This study adhered to the tenets of the Declaration of Helsinki, and approval for this research was obtained from the institutional review board of the Boston University Medical Campus. Informed consent was obtained, after explanation of the nature and possible consequences of the study, from consecutive patients undergoing excision of ocular surface lesions at Boston Medical Center by a single surgeon between July 2016 and August 2017. After excision of each lesion, the surgeon used a 1 or 2 mm dermatologic biopsy punch to separate a central portion of each excised lesion, leaving the lateral margins intact. The peripheral portion was immediately fixed in 10% formalin. The central portion was placed in sterile phosphate buffered saline (PBS) with 2% bovine serum albumin (BSA) on ice and imaged as described below. Immediately after imaging, the central specimen was placed in 10% formalin. The peripheral and central portions of each lesion then were sent to the Boston Medical Center clinical pathology laboratory for routine processing and histologic diagnosis.

Instrumentation and Imaging Technique

The instrumentation and method of ISOCT have been described previously.[15,17] Briefly, a fiber-based Fourier-domain OCT configuration was implemented. A supercontinuum source provided laser illumination in the visible light range. A house-made spectrometer collected OCT signals in the 530 to 600 nm spectral range. After OCT signal acquisition, a short time Fourier transform (STFT) was performed to generate four-dimensional (4D) data $I(x,y,z,\lambda)$, where x, y, z denotes 3D Cartesian space and λ denotes wavelength. The full width half maximum (FWHM) of the spectral window in STFT is approximately 10 nm. Three quantitative IS-OCT

markers were derived from the 4D dataset, D, μ_b, and μ_s. D is a physical parameter defining the tissue ultrastructural heterogeneity, and higher D conceptually represents higher tissue compaction and aggregation. D is calculated by fitting the spectra from the imaged area by a power law with the relation of $I \infty \lambda^{4-D}$. μ_b (mm^{-1}) is determined by the reflectance, and is a compound marker that is determined by tissue mass density and the heterogeneity. μ_s (mm^{-1}) measures the signal decay along the penetration depth by $I \infty I_0 \exp(-\mu_s z)$. The area of each tissue imaged was approximately 1×1 mm^2 or 2×2 mm^2 depending on the size of the biopsy, and to a depth of approximately 0.3 to 0.4 mm. The measurements of μ_b and D were taken from the superficial 50 µm of each tissue, and primarily included the conjunctival epithelium of each specimen. The measurement of μ_s was taken within a depth range of 0.3 mm from the tissue surface.

2P-AF was performed after ISOCT using a commercially available Zeiss LSM 710-Live Duo Confocal microscope (Carl Zeiss Meditec, Dublin, CA). NADH and FAD autofluorescence signals were collected by 760 and 860 nm excitation, respectively. At each channel, the 3D image was acquired in x, y, and z dimensions of $0.2 \times 0.2 \times 0.04$ mm, respectively. The superficial 50 µm of each specimen, primarily comprised of epithelium, was imaged. 2P-AF was performed subsequently and immediately after ISOCT. The entire measurement time was completed within 2 hours of excision.

Correlation of ISOCT and 2P-AF Findings to Histologic Diagnosis

The individuals taking images and performing ISOCT or 2P-AF analysis were masked to the clinical or pathologic diagnosis of each tissue. Histopathologic diagnosis of each specimen was made by a single board-certified ophthalmic pathologist as part of the standard of care. Hematoxylin and eosin staining of tissue, as well as Ki67 immunohistochemistry, were performed according to the standard of care practices of the Boston Medical Center clinical pathology laboratory. Specimens were grouped by final pathologic diagnosis into benign or premalignant (combined dysplastic and/or malignant) categories. ISOCT markers D, μ_b, and μ_s were averaged for the specimens within each tissue category. The average D, μ_b, and μ_s values then were compared between the two categories. 3D ISOCT heat map images also were constructed, and these were qualitatively compared to 2D histologic images. For 2P-AF analysis, the average NADH autofluorescence, average FAD autofluorescence, and the average FAD/(FAD+NADH) (redox ratio) autofluorescence signals within the epithelium were compared between the two tissue categories. Standard error of mean also was calculated for each averaged data set.

Statistical Analysis

The independent t-test was used to determine if differences in quantitative ISOCT markers and 2P-AF signals between benign or premalignant tissues were statistically significant. $P < 0.05$ was considered statistically significant.

Results

Fourteen conjunctival excisional biopsy specimens of 13 patients were analyzed by ISOCT. The clinical and histologic diagnoses of each lesion are summarized in the Table. A squamous papilloma with areas of mild-to-moderate dysplasia was categorized as premalignant due to the presence of dysplasia. Two lesions diagnosed by histology as squamous cell carcinoma in situ (on the OSSN spectrum) were categorized as malignant. The remaining 11 lesions were categorized as benign. Nine of these 11 benign lesions were pterygium. Representative examples of ISOCT images are shown in Figure 1a to 1c, in parallel with hematoxylin and eosin (H&E)–stained histologic sections (Figs. 1d–f). A visual 3D heat map of D, a marker associated with ultrastructural compaction, shows an increase in D in malignant and premalignant conjunctival epithelium (Figs. 1g–i).

The ISOCT marker D was 2.2-fold higher in premalignant compared to benign lesions (4.27 ± 0.28 vs. 1.92 ± 0.26, $P = 9 \times 10^{-4}$; Fig. 2). The individual values for each specimen are shown in the Table. There were no significant differences between μ_s and μ_b between premalignant and benign groups (Fig. 2).

For 2P-AF analysis, three lesions were excluded because two-photon microscopy was not available at collection. Of the 11 included lesions, nine were benign, one was premalignant, and one was malignant (Table). Representative images of NADH and FAD autofluorescence for each lesion category are shown in Figure 3.

Ki67 immunostaining was performed as part of standard clinical diagnostic analysis by the Boston Medical Center pathology laboratory in suspected

Table. ISOCT and 2P-AF Data per Specimen

Patient	Age/ Sex	Eye	Clinical Diagnosis	Histological Diagnosis	Category	ISOCT			2P-AF		
						D	μ_s (mm^{-1})	μ_b (mm^{-1})	NADH	FAD	Redox
1	36/M	Left	Pterygium	Pterygium	Benign	1.85	0.011	0.407	14.37	20.09	0.58
2	60/F	Left	Pterygium	Pterygium	Benign	0.60	0.014	0.596	4.65	2.83	0.39
		Right	Pterygium	Pterygium	Benign	1.94	0.018	0.662	1.51	1.52	0.50
3	44/M	Right	Pterygium	Pterygium	Benign	2.19	0.017	0.604	2.51	2.44	0.49
4	33/M	Right	Pterygium	Pterygium	Benign	2.65	0.016	0.680	3.59	2.70	0.43
5	60/F	Right	Pterygium	Pterygium	Benign	2.16	0.016	0.642	2.85	2.61	0.48
6	56/M	Right	Pterygium	Pterygium	Benign	0.10	0.007	0.499	4.53	4.46	0.50
7	28/M	Left	Pterygium	Pterygium	Benign	1.83	0.017	0.665	4.16	4.11	0.50
8	70/M	Left	Map biopsy, previously excised PAM with severe atypia and melanoma in situ	Limbal conjunctiva with stromal fibrosis	Benign	2.93	0.016	0.693	10.26	2.67	0.21
9	73/M	Right	Corneal intraepithelial neoplasia (OSSN)	Pterygium, benign melanosis and microcalcifications	Benign	2.64	0.015	0.406	NA	NA	NA
10	62/F	Left	Map biopsy, s/p excision of malignant melanoma	Conjunctiva, no evidence of PAM or malignancy	Benign	2.22	0.010	0.529	NA	NA	NA
11	61/M	Right	Papilloma	Squamous papilloma with mild dysplasia	Premalignant	3.73	0.013	0.492	25.98	3.31	0.11
12	87/M	Left	OSSN	Squamous cell carcinoma in situ	Malignant	4.38	0.012	0.533	14.22	1.68	0.11
13	70/M	Left	OSSN	Squamous cell carcinoma in situ, early stromal invasion cannot be excluded	Malignant	4.69	0.009	0.672	NA	NA	NA

PAM, primary acquired melanosis; s/p, status post.

malignant tissues only, and showed a high level of epithelial cell proliferation in the squamous papilloma and squamous carcinoma tissues (Figs. 3g, 3h).

2P-AF analysis of NADH and FAD autofluorescence suggested 3.7-fold higher NADH autofluorescence in premalignant versus benign lesions (20.10 ± 5.88 vs. 5.38 ± 1.40, $P = 0.23$; Fig. 4a), and 0.51-fold lower FAD autofluorescence in premalignant versus benign lesions (2.50 ± 0.81 vs. 4.83 ± 1.93, $P = 0.30$; Fig. 4b), but neither difference was statistically significant. However, when calculating a redox ratio (FAD/FAD+NADH), there was a statistically significant 0.24-fold lower redox ratio in premalignant versus benign lesions (0.11 ± 0.005 vs. 0.45 ± 0.04, $P = 1.08\times10^{-5}$; Fig. 4c).

Discussion

In this pilot study of ISOCT imaging of ocular surface lesions, we found that the ISOCT marker D was consistently higher in ocular surface tissue harboring malignancy or dysplasia, specifically in squamous cell carcinoma in situ and dysplastic papilloma. These results are in line with previous studies reporting higher D in the early stages of

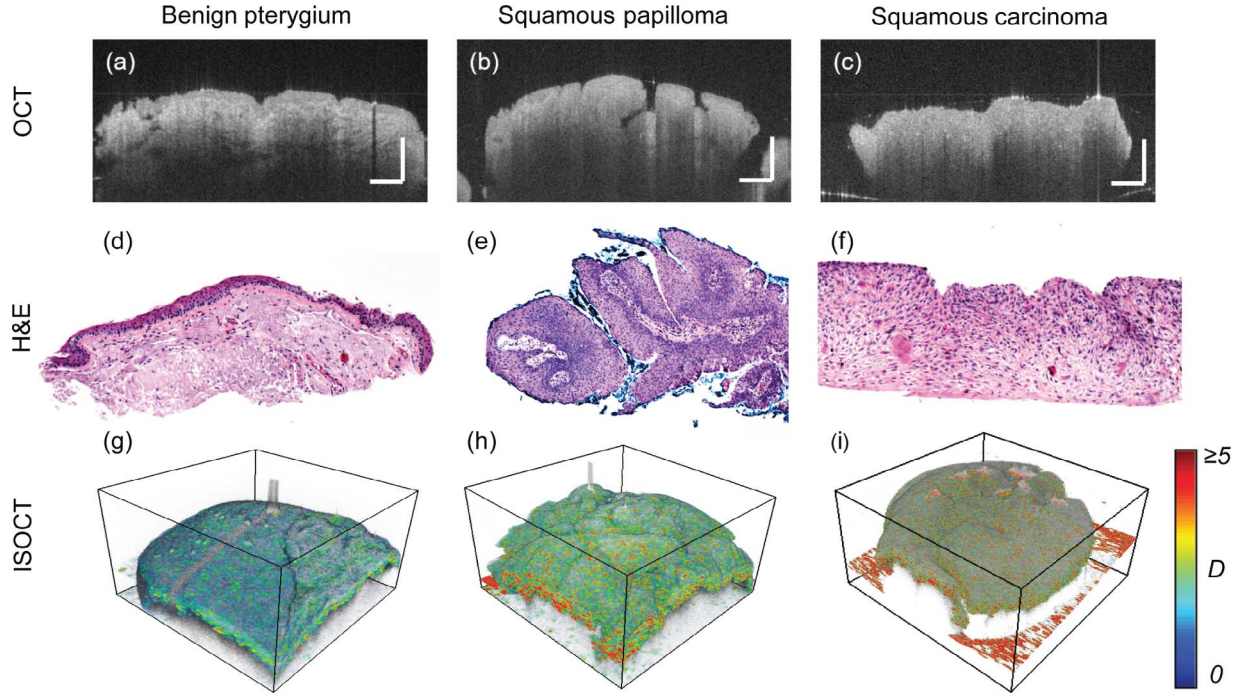

Figure 1. Qualitative representation of ISOCT ultrastructural marker *D* in ocular surface lesions. Representative OCT images and H&E-stained sections (courtesy of Nora Laver, MD and the Boston Medical Center pathology laboratory) are compared to ISOCT 3D intensity maps of ultrastructural marker *D* in pterygium (a, d, g), dysplastic conjunctival papilloma (b, e, h), and squamous cell carcinoma (c, f, i). *D* is relatively low in pterygium (g), higher in dysplastic conjunctival papilloma (h), and highest in squamous cell carcinoma (i). *OCT scale bar*: 200 μm. H&E images are at ×10.

various cancer types, including colon, pancreas and lung cancer.[17,19–21] Thus, our results suggested that *D* is a sensitive marker of malignancy or malignant potential in the ocular surface as well. Higher *D* values indicated more compact and condensed structure, and have been correlated with increasing chromatin compaction, as well as with increasing collagen crosslinking.[16,22] Collagen crosslinking has been implicated in the development and invasion of malignant tumors.[23] Lysyl oxidase, which catalyzes the crosslinking of collagen, is overexpressed in many cancers.[24] The higher *D* associated with malignant or

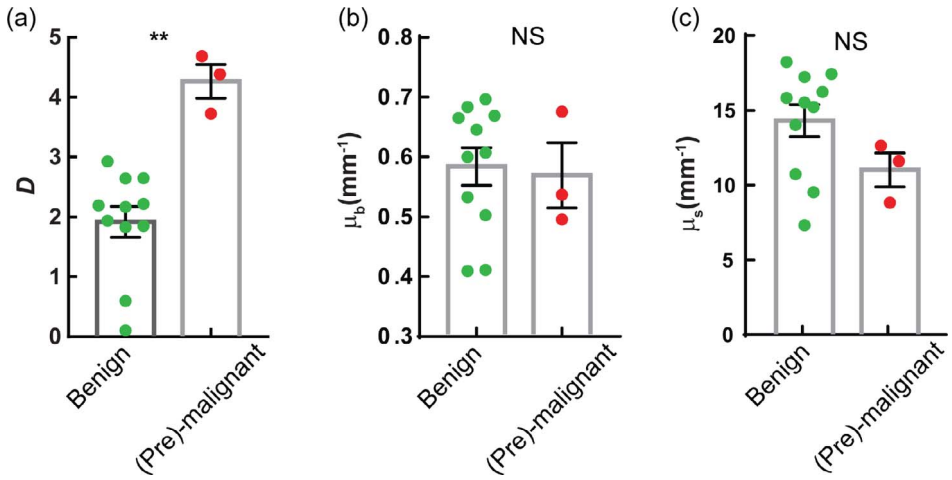

Figure 2. Quantitative comparison of ISOCT markers in benign versus premalignant ocular surface lesions. *D* is significantly higher in premalignant (*red*, $n = 3$) versus benign lesions (*green*, $n = 11$) (a). μ_b (b) and μ_s (c) are not significantly different between the two groups. $P < 0.001$ (**), not significant (ns). *Error bars*: SEM.

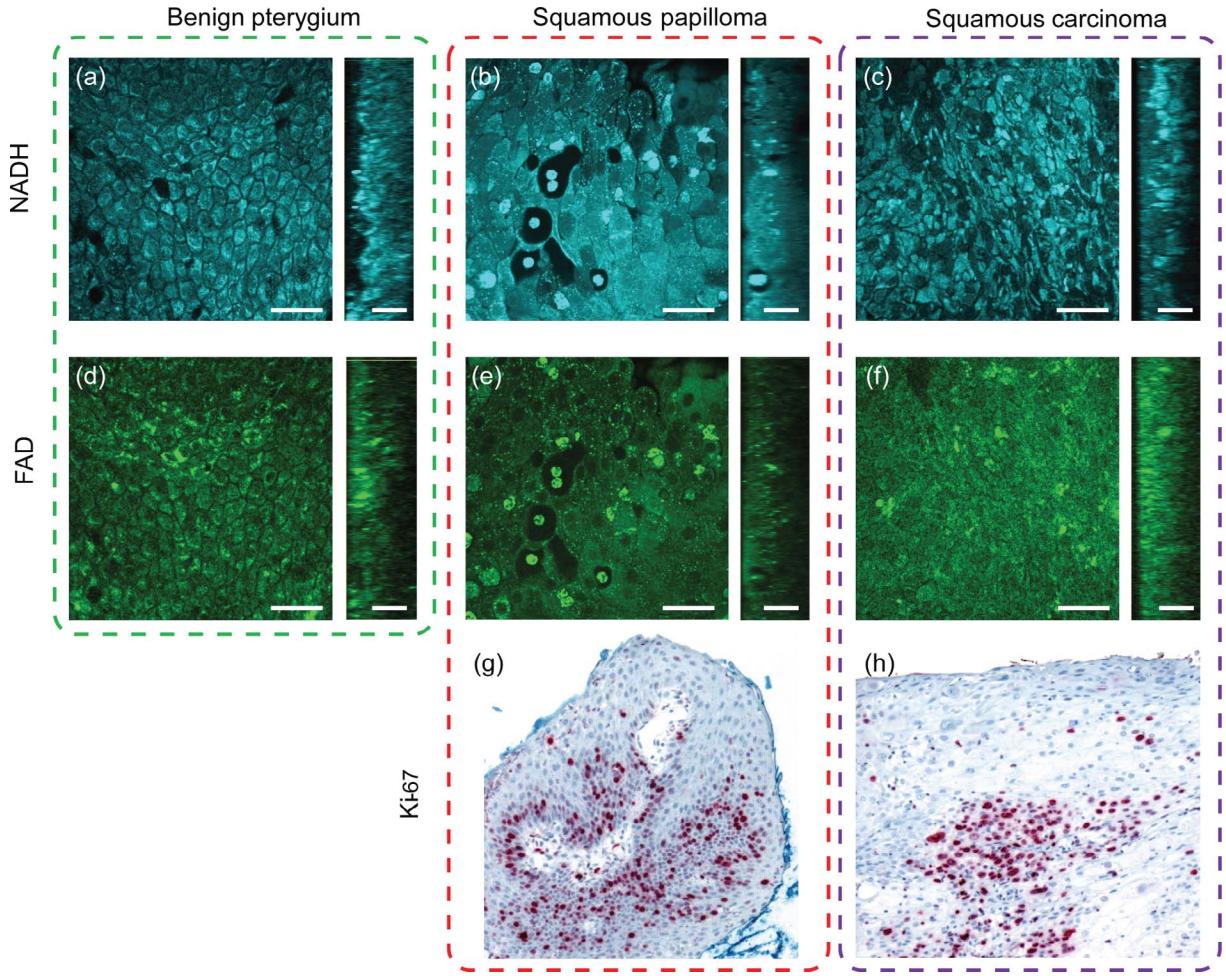

Figure 3. Qualitative representation of 2P-AF metabolic markers and cellular proliferation in ocular surface lesions. Representative 2P-AF NADH and FAD autofluorescence images of pterygium (a, d), dysplastic squamous papilloma (b, e), and squamous cell carcinoma (c, f). *Scale bar*: 40 μm. Ki67 immunohistochemistry shows many positive cells (*magenta*) in dysplastic squamous papilloma (g) and squamous cell carcinoma (h) (courtesy of Nora Laver, MD and the Boston Medical Center pathology laboratory).

premalignant tissues could potentially involve changes in these properties.

In addition, in our analysis of ocular surface lesions by 2P-AF, we found that the redox ratio was significantly lower in malignant and dysplastic conjunctival lesions compared to benign lesions. A lower redox ratio suggests a shift in cellular metabolism from oxidative phosphorylation to glycolysis, and cancers are known to display the Warburg effect, whereby malignant cells increase anaerobic respiration, resulting in a lower redox ratio, while maintaining a high metabolic demand.[25,26] The Warburg effect is the basis for how positron emission tomography (PET) scans noninvasively detect malignant tumors.[27] The malignant and dysplastic lesions that we examined displayed a high degree of proliferation, as evidenced by the density of Ki-67–positive cells (Fig. 3). Thus, the combination of high proliferative rate and lower redox ratio suggests that the Warburg effect could be present in squamous cell carcinoma and dysplastic squamous papilloma of the conjunctiva.

Our study did not address whether ISOCT or 2P-AF could be useful in distinguishing between invasive and noninvasive forms of ocular surface malignancy. Theoretically, if the area analyzed included the stroma, deep scleral invasion could be detectable; however, this would not be practical in lesions with thickened epithelium due to issues of light penetration, as significant shadowing begins to occur at a depth of approximately 200 to 300 μm with ISOCT (data not shown), and the maximum depth of penetration of 2P-AF is 50 μm. For the purpose of this study, we limited our analysis to the superficial 50

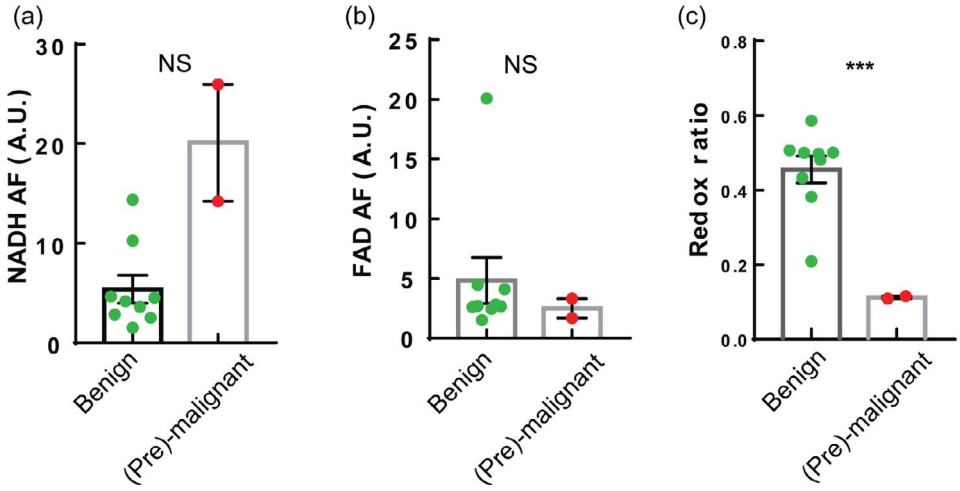

Figure 4. Quantitative comparison of 2P-AF metabolic markers in benign versus premalignant ocular surface lesions. Comparison of NADH auto-fluorescence (a), FAD autofluorescence (b), and redox ratio (FAD/FAD+NADH) (c) between benign (*green*, $n = 9$) and premalignant (*red*, $n = 2$) lesions. The redox ratio was significantly lower in premalignant versus benign lesions. $P = 1 \times 10^{-5}$ (***), not significant (ns), arbitrary unit (A.U.), auto-fluorescence (AF). *Error bars*: SEM.

μm of each lesion because we wanted to be as consistent as possible in comparing the lesions to each other and between modalities (ISOCT vs. 2P-AF). By using a depth of 50 μm, we also limited the analysis to the epithelium in all samples, and avoided capturing stroma in the thinner lesions. In future studies, it will be important to further analyze the effect of modifying the depth of analysis, and whether ISOCT may be able to help distinguish invasive from noninvasive cancer. However, we anticipate that ISOCT in particular will be more useful for detecting early signs of malignancy, rather than for detecting signs of stromal invasion.

The small sample size, particularly of malignant lesions, is certainly a major limitation of this pilot study. Furthermore, the types of malignant lesions we encountered were limited to ocular surface squamous neoplasia. Thus, we are not able to conclude whether ISOCT or 2P-AF could help detect malignant potential in melanocytic lesions. Nevertheless, to our knowledge, our results are the first to demonstrate that ISOCT and 2P-AF can be used successfully to image conjunctival lesions, and that significant differences between lesion types can be detected. ISOCT has been safely and effectively used to image human eyes in vivo, and studies are now underway to use ISOCT in patients to detect differences in ocular surface lesions. The early results from this study suggest that ISOCT and intrinsic autofluorescence imaging has the potential to be clinically useful for the sensitive noninvasive detection and grading of ocular surface malignancies when eventually applied in vivo.

Acknowledgments

The authors thank Nora Laver, MD, for contributing all of the H&E and Ki67-stained histologic section images, and thank Sharmila Masli, PhD, and Lilla Simon for their assistance.

Supported by the Boston University Clinical and Translational Science Institute (CTSI) program through National Institutes of Health (NIH; Bethesda, MD) CTSI Grant 1UL1TR001430 to Hyunjoo Jean Lee, and National Eye Institute Grant R21EY029412 to Hyunjoo Jean Lee (ORCID: 0000-0002-2814-6664) and Ji Yi (ORCID: 0000-0001-6583-7192).

Disclosure: **H.J. Lee**, None; **L. Zhang**, None; **S. Zhang**, None; **J. Yi**, Biological tissue analysis by inverse spectroscopic optical coherence tomography, U.S. Patent 9,678,007 (P)

References

1. Shields CL, Chien JL, Surakiatchanukul T, Sioufi K, Lally SE, Shields JA. Conjunctival tumors: review of clinical features, risks, biomarkers, and outcomes–the 2017 J. Donald M. Gass lecture. *Asia Pac J Ophthalmol (Phila)*. 2017;6:109–120.

2. Shields CL, Shields JA. Ocular surface squamous neoplasia: from blue skies to blue dyes–we still need our ophthalmic pathologists. *JAMA Ophthalmol*. 2015;133:1321–1322.
3. Moshirfar M, Khalifa YM, Kuo A, Davis D, Mamalis N. Ocular surface squamous neoplasia masquerading as superior limbic keratoconjunctivitis. *Middle East Afr J Ophthalmol*. 2011;18:74–76.
4. Kim JW, Abramson DH. Topical treatment options for conjunctival neoplasms. *Clin Ophthalmol*. 2008;2:503–515.
5. Nanji AA, Sayyad FE, Karp CL. Topical chemotherapy for ocular surface squamous neoplasia. *Curr Opin Ophthalmol*. 2013;24:336–342.
6. Shah SU, Kaliki S, Kim HJ, Lally SE, Shields JA, Shields CL. Topical interferon alfa-2b for management of ocular surface squamous neoplasia in 23 cases: outcomes based on American Joint Committee on Cancer classification. *Arch Ophthalmol*. 2012;130:159–164.
7. Shields CL, Kaliki S, Kim HJ, et al. Interferon for ocular surface squamous neoplasia in 81 cases: outcomes based on the American Joint Committee on Cancer classification. *Cornea*. 2013;32:248–256.
8. Kanavi MR, Hosseini SB, Aliakbar-Navahi R, Aghaei H. Impression cytology in a series of clinically diagnosed ocular surface melanocytic lesions. *J Ophthal Vis Res*. 2017;12:17–22.
9. Paridaens AD, McCartney AC, Curling OM, Lyons CJ, Hungerford JL. Impression cytology of conjunctival melanosis and melanoma. *Br J Ophthalmol*. 1992;76:198–201.
10. Kieval JZ, Karp CL, Abou Shousha M, et al. Ultra-high resolution optical coherence tomography for differentiation of ocular surface squamous neoplasia and pterygia. *Ophthalmology*. 2012;119:481–486.
11. Nanji AA, Sayyad FE, Galor A, Dubovy S, Karp CL. High-resolution optical coherence tomography as an adjunctive tool in the diagnosis of corneal and conjunctival pathology. *Ocul Surf*. 2015;13:226–235.
12. Shousha MA, Karp CL, Perez VL, et al. Diagnosis and management of conjunctival and corneal intraepithelial neoplasia using ultra high-resolution optical coherence tomography. *Ophthalmology*. 2011;118:1531–1537.
13. Shousha MA, Karp CL, Canto AP, et al. Diagnosis of ocular surface lesions using ultra-high-resolution optical coherence tomography. *Ophthalmology*. 2013;120:883–891.
14. Alzahrani YA, Kumar S, Abdul Aziz H, Plesec T, Singh AD. Primary acquired melanosis: clinical, histopathologic and optical coherence tomographic correlation. *Ocul Onc Pathol*. 2016;2:123–127.
15. Yi J, Backman V. Imaging a full set of optical scattering properties of biological tissue by inverse spectroscopic optical coherence tomography. *Opt Lett*. 2012;37:4443–4445.
16. Spicer GL, Azarin SM, Yi J, et al. Detection of extracellular matrix modification in cancer models with inverse spectroscopic optical coherence tomography. *Phys Med Biol*. 2016;61:6892–6904.
17. Yi J, Radosevich AJ, Stypula-Cyrus Y, et al. Spatially resolved optical and ultrastructural properties of colorectal and pancreatic field carcinogenesis observed by inverse spectroscopic optical coherence tomography. *J Biomed Opt*. 2014;19:36013.
18. Kolenc OI, Quinn KP. Evaluating cell metabolism through autofluorescence imaging of NAD(P)H and FAD. *Antiox Redox Signal*. 2019;30:875–889.
19. Radosevich AJ, Mutyal NN, Rogers JD, et al. Buccal spectral markers for lung cancer risk stratification. *PLoS One*. 2014;9:e110157.
20. Roy HK, Turzhitsky V, Kim Y, et al. Association between rectal optical signatures and colonic neoplasia: potential applications for screening. *Cancer Res*. 2009;69:4476–4483.
21. Turzhitsky V, Liu Y, Hasabou N, et al. Investigating population risk factors of pancreatic cancer by evaluation of optical markers in the duodenal mucosa. *Dis Markers*. 2008;25:313–321.
22. Yi J, Stypula-Cyrus Y, Blaha CS, Roy HK, Backman V. Fractal characterization of chromatin decompaction in live cells. *Biophys J*. 2015;109:2218–2226.
23. Levental KR, Yu H, Kass L, et al. Matrix crosslinking forces tumor progression by enhancing integrin signaling. *Cell*. 2009;139:891–906.
24. Wang TH, Hsia SM, Shieh TM. Lysyl oxidase and the tumor microenvironment. *Int J Mol Sci*. 2016;18:E62.
25. DeBerardinis RJ, Lum JJ, Hatzivassiliou G, Thompson CB. The biology of cancer: metabolic reprogramming fuels cell growth and proliferation. *Cell Metab*. 2008;7:11–20.
26. Wu W, Zhao S. Metabolic changes in cancer: beyond the Warburg effect. *Acta Bioch Biophys Sinica*. 2013;45:18–26.
27. Bensinger SJ, Christofk HR. New aspects of the Warburg effect in cancer cell biology. *Sem Cell Devel Biol*. 2012;23:352–361.